buildings

MDPI

Article

A Method for Determination of Moment Contribution Ratio under Foundation Rotation in Shear Wall-Frame Systems

Kanat Burak Bozdogan [1,*] and Erdinc Keskin [2]

[1] Department of Civil Engineering, Canakkale Onsekiz Mart University, Canakkale 17020, Turkey
[2] Department of Civil Engineering, Kırklareli University, Kırklareli 39750, Turkey; erdinckeskin@klu.edu.tr
* Correspondence: kbbozdogan@comu.edu.tr

Abstract: In shear wall-frame systems, the foundation rotation that may occur under the shear walls changes the displacements and interstory drift ratios and changes the internal force distribution. This study investigates the effect of foundation rotations under shear walls on internal force distribution in shear-frame systems. The originality of the study lies in considering parabolic loads and dynamic analysis (first mode), in addition to static uniform or triangular distributed loads, when determining the shear wall moment contribution ratio under the influence of foundation rotation. The shear wall contribution ratio, a key parameter in many earthquake codes, is defined as the ratio of the sum of bending moments taken by the shear walls at the base to the overturning moment. It plays a crucial role in determining the building's behavior. Depending on this ratio, the load-reduction coefficient is changed. This study investigates the effect of foundation rotation on the moment distribution at the base for three different static load cases and the first mode in the dynamic analysis. The multi-story building is modeled as an equivalent sandwich beam. The moment contribution ratio (MCR) was calculated with the help of analytical solutions of the differential equations written for three different load cases in static conditions, and graphs were created for practical use directly calculating the MCR. In the methodology of the study, the initial step involves the calculation of the equivalent sandwich beam stiffness parameters and the foundational rotational spring. Subsequent to these calculations, the MCR values can be directly obtained with the help of graphs. This approach facilitates the rapid and practical determination of the MCR and can be used in the preliminary sizing phase to eliminate possible errors in the data entry of software that performs detailed analysis. In addition, in the presented study, it has been shown that taking a single mode into account is sufficient when calculating MCR values in dynamic analysis.

Keywords: moment contribution ratio; shear wall frame; foundation rotation; equivalent sandwich beam model; static analysis; dynamic analysis; finite element method

Citation: Bozdogan, K.B.; Keskin, E. A Method for Determination of Moment Contribution Ratio under Foundation Rotation in Shear Wall-Frame Systems. *Buildings* **2024**, *14*, 467. https://doi.org/10.3390/buildings14020467

Received: 21 December 2023
Revised: 30 January 2024
Accepted: 6 February 2024
Published: 7 February 2024

1. Introduction

During an earthquake, the interaction between foundation soils and the building plays a crucial role in determining the structure's response to seismic forces. The foundation soils act as both a filter and a transmitter of the seismic shaking, transferring it to the building. Simultaneously, the soil bears the vibrations induced by the building and transmits them back into the depths of the soil. This dynamic exchange between the structure and the supporting soil underscores the importance of considering their inter-play in the design process [1–4].

A noteworthy phenomenon observed, especially in the foundations of multi-story buildings during significant earthquakes, is the occurrence of unforeseen foundation rotations. These rotations, stemming from the complex interaction between the building and the underlying soil, can have a profound impact on the dynamic characteristics of the structure. Neglecting to account for these foundation rotations in the design phase can

lead to significant oversights in predicting the total displacements that the structure may experience during seismic events [5–8].

In essence, the seismic performance of a structure is intimately tied to the intricate relationship between the building and its foundation [9,10]. Engineers must carefully assess and incorporate the potential for foundation rotations into the design process to ensure the structural integrity and resilience of buildings in the face of seismic challenges. By acknowledging the dynamic interdependence of soil and structure, engineers can implement measures that enhance the earthquake resistance of buildings, ultimately contributing to the safety and stability of the built environment.

Forcellini [11] extensively explored soil–structure interaction (SSI) effects using advanced numerical simulations despite their time-consuming nature. When comparing SSI models with fixed-base counterparts, the study identified two key effects: period elongation and damping increase. The study introduced numerical models to create calibrated fixed-based models, enabling intricate SSI analyses. The proposed framework for evaluating SSI with equivalent fixed-based models was validated through nonlinear dynamic numerical simulations, employing Opensees to replicate nonlinear scenarios with considerations for hysteretic materials and advanced soil models.

Carbonari et al. [12] examined the impact of soil–structure interaction on coupled wall–frame structures with pile foundations during moderate earthquakes. Employing a linear finite element procedure in the frequency domain, the analysis considered soil–pile interaction and radiation damping for a comprehensive dynamic interaction study. This approach accommodated the actual deformability of the soil foundation system and adjusted input motion due to the embedded foundation. The study utilized local response analysis to derive free field motion, accounting for site amplification. Investigating compliant pile foundations, the procedure assessed the seismic damageability of coupled wall-frame systems under varying soil profiles and real accelerograms. Results, including displacements, interstory drifts, accelerations, and stress resultants, were compared with a traditional fixed-base model, highlighting the importance of complete soil–structure interaction analyses for accurate system behavior evaluation.

Carbonari et al. [13] aimed to explore soil–structure interaction effects on the seismic response of modern seismic provisions-designed, pile-founded coupled wall-frame structures. The analysis method, rooted in the substructure approach, was refined, emphasizing the modeling of pile group foundations. Nonlinear inertial interaction analysis, conducted in the time domain using a finite element superstructure model, employed lumped parameter models to replicate frequency-dependent compliance of soil-foundation systems. Assessing soil–structure interaction effects involved a realistic case study of a 6-story, 4-bay wall-frame structure on pile foundations, exploring various two-layered soil deposits with different properties. Simulated earthquakes facilitated comparisons between compliant and fixed base models, focusing on displacements, base shears, and ductility demand. The study investigated the evolution of dissipative mechanisms and shear redistribution between the wall and frame under earthquakes of increasing intensity, emphasizing the significance of both kinematic and inertial interaction on foundations.

Santrac et al. [14] outlined the efforts to strengthen the foundations of the Cathedral of St. Theresa of Avila's towers in Subotica and the resulting damages. Through an examination of historical data, recorded damages, geodetic measurements, and insights gained from rehabilitation efforts, the study highlighted a complex interaction problem between a substantial structure and an inadequately load-bearing foundation.

Jiménez and Dias [15] examined the influence of dynamic characteristics on structures by analyzing buildings of varying heights (three to seven stories). The study utilized a linear elastic perfectly plastic model with a Mohr–Coulomb failure criterion to represent soil behavior. It provided values for maximum lateral displacements, interstory drifts, shear forces distribution in buildings, and foundation rocking. Comparing efforts and displacements in different foundation systems, the results highlighted the significant impact of support conditions on the seismic response, efforts, and displacements in rigid elements,

depending on the foundation system. Toe-level efforts in rigid elements were highly influenced by support conditions, with only a slight influence from the head connection.

Oz et al. [16], post-earthquake reconnaissance, highlighted existing buildings' notably low seismic performance, especially those on weak soils, indicating the adverse impact of soil–structure interaction. This investigation involved constructing nonlinear models for 40 Turkish buildings, considering fixed-base and varying soil conditions (stiff, moderate, and soft). Categorizing buildings as old and new based on pre- and post-1998 Turkish Earthquake codes, different soil conditions were reflected using the substructure method. Inelastic deformation demands were obtained through nonlinear time history analysis and 20 real acceleration records. Results revealed that soil–structure interaction significantly affects the seismic response of old buildings, particularly in soft soil cases, with a notable increase in drift demands in the first stories.

Bariker and Kolathayar [17] focused on the safety of high-rise buildings supported by pile-mat systems, requiring robustness against lateral loads from earthquakes, wind, dredging, and machine vibrations, along with increased axial loads. The innovative finned pile foundation system, proven to withstand 65% to 80% higher lateral loads than conventional pile systems, was explored through a series of SSI analyses on a 25-story building. Utilizing ABAQUS software (Version 6.21), seismic responses were assessed for different fin lengths (0.2 Lp, 0.4 Lp, 0.6 Lp, and 0.8 Lp) and compared with a conventional piled mat. Results showed a significant reduction in vibrations and seismic effects with FP-Mats, suggesting 0.6 Lp as the optimum fin length for seismic performance and construction efficiency.

Wang et al. [18] underscored the reliance of most regional seismic damage assessment (RSDA) methods on the rigid-base assumption, leading to factual errors by overlooking SSI. Addressing this challenge, the study proposed a one-dimensional convolutional neural network (1D-CNN) model to efficiently predict the impact of SSI on interstory drifts and base shear forces in RC frame buildings. Using an experimentally validated finite element model, the study established a database with 1380 pairs of fixed-base and soil-supported structures under earthquake loading. Training the 1D-CNN model on this dataset revealed its superior performance, with absolute prediction errors for SSI influence coefficients within 9.3% and 11.7% for maximum base shear and interstory drift, respectively, in 80% of testing cases.

Shehata et al. [19] proposed a new methodology for time–domain analysis of buildings on raft foundations, incorporating soil–structure interaction. The sub-structuring technique divided the structure into the superstructure and underlying soil. While any numerical method could model the superstructure, the study employed the boundary element method (BEM) to consider the actual interaction between columns and slabs. Dynamic loads were treated as earthquake acceleration records transformed into equivalent loads on superstructure floors. The substructure was analyzed using the dual reciprocity boundary element method in a closed domain. An innovative iterative coupling technique was suggested to reduce computational effort.

Ali et al. [20] explored cost-effective seismic design methods, emphasizing SSI benefits over fixed-base designs. While popular finite element methods for SSI incurred high costs and long analyses, low-cost alternatives often neglected ground properties. This research advocated a machine learning approach for efficient and comprehensive structural analysis. Artificial neural networks and support vector machines were employed to assess SSI effects on seismic responses across diverse earthquake scenarios.

The study by Gan et al. [21] investigated dynamic structure–soil–structure interaction (SSSI) involving three adjacent structures with pile–raft foundations in a viscoelastic half-space under earthquake excitation. The effects of SSSI were explored by considering factors like the clear distance between structures, structure types, heights, and first natural periods. Numerical simulations revealed significant variations in SSSI effects, and the seismic response of structures is found to depend on structural characteristics rather than their locations.

Forcellini [22] assessed seismic risk and resilience in structures, emphasizing the impact of base isolation. The research explored how losses from earthquakes can be minimized by implementing base isolation strategies, considering soil deformability and SSI. Through numerical simulations, various isolated configurations on diverse soil conditions were evaluated, with computed resilience serving as a reference for comparing isolation models.

Lanes et al. [23] presented a numerical methodology for analyzing frame structures on footing foundations subjected to slow strains from consolidation settlements. Using the boundary element method with the Mindlin fundamental solution, they calculated displacements resulting from pressure bulbs' interference on the foundation. The study incorporated the rheological Kelvin–Voigt model for soil–structure interactions, applying Terzaghi's theory of consolidation to match displacement time curves. The rheological model was coupled with structural nonlinear geometric effects through an iterative process. Results aligned with predicted settlement effects, emphasizing the potential for significant increases in specific regions of the building structure due to the gradual distribution of efforts.

The study by Zhang and Far [24] explored the impact of SSI on high-rise frame-shear wall buildings with multiple basements. Traditionally, structures were assumed rigid, neglecting SSI in design for perceived seismic benefits. However, recent findings suggested potential drawbacks. The research, validated through shaking table tests, employed a finite-element model to analyze various superstructure and sub-structure parameters. Results showed that increased subsoil stiffness significantly amplifies base shear, and rising foundation rotation increased interstory drifts while reducing base shears. SSI generally amplifies interstory drifts, but its effects on base shear vary with foundation types and soil conditions. The study provided minimum base shear ratios, considering the SSI reduction effect, for structures with different foundation types.

The study by Zang and Far [25] challenged the conventional assumption that SSI is universally beneficial during seismic loading. Using an enhanced numerical model in ABAQUS, the research focused on high-rise frame-core tube structures and investigated the impact of SSI. Analyzing buildings on soil class Ee according to Australian Standards, the seismic responses of 20, 30, and 40-story structures under four earthquake records were examined. Findings revealed that SSI significantly affects the seismic behavior of these structures, increasing lateral deflections and interstory drifts while decreasing story shear forces. Notably, seismic responses differed significantly between near and far field earthquakes in soil–structure systems.

Colina et al. [26] examined the effect of foundation rotation on the behavior of a two-story reinforced concrete frame. In the study conducted by applying harmonic load, it was emphasized that foundation rotation may create additional torsion effects in buildings.

Koboevic and Murugananthan [27] investigated the effect of foundation rotation on steel-braced frame buildings based on the Canadian seismic code and emphasized that foundation rotation increases the displacements and interstory drifts. Therefore, this increase should be taken into account in the calculation of displacements.

Adebar [28], stating that foundation rotations increase the displacement of buildings, proposed a simple method for calculating the displacement and relative story drifts of buildings under the influence of foundation rotation. The method he proposed was based directly on hand calculation.

Kakhki et al. [29] examined the progressive collapse of shear wall-frame systems by taking into account the structure–soil interaction. At the end of the study, it was shown that the foundation thickness was the most critical parameter affecting the behavior.

Sadek et al. [30] investigated the effect of the nonlinear behavior of the ground on shear walls, and, as a result, it was stated that the assumption that the ground behaves elastically in the structure–soil interaction cannot adequately represent the behavior under earthquake loads. Therefore, it was argued that the nonlinear behavior of the ground should be taken into account in the analyses.

Mohsenian et al. [31] underlined the potential impact of increased weight and stiffness on tunnel-form buildings during seismic events. To address these challenges, the study emphasized the critical importance of accounting for SSI in the modeling process. In conclusion, the study suggested that in seismically active areas with soft soil, SSI effects could impede tall buildings from achieving predefined performance standards.

Alexandre et al. [32] introduced a model that facilitates the coupled analysis of concrete and soil, incorporating time-dependent aspects such as hardening, creep, shrinkage, cracking of concrete, and soil consolidation. The one-dimensional finite element modeling, utilizing Kelvin chains for time-dependent behavior, demonstrated significant changes in the effects of SSI, particularly in the study of a reinforced concrete continuous beam on consolidating clay.

Tang et al. [33] investigated the redistribution of internal forces and the development of plastic hinges in a multi-story building system with foundations at varying elevations, considering torsional effects. The results uncovered significant redistributions of base and story shear forces, with a more pronounced internal force redistribution along the slope direction. As the seismic intensity increases, the damage was shown to be displaced from upper floors to those beneath the upper embedding point, particularly affecting elements above this embedding point.

Mishra and Samanta [34] investigated the structural response of nine-story buildings with and without shear walls on soft soil, specifically in the seismic region of Patna, India. Analyzing various conditions, including fixed and flexible bases, the research concluded that shear and infill walls play a crucial role in reducing seismic responses, while base flexibility increases vulnerability. Additionally, the study highlighted the significance of aspect ratio in determining displacement ductility and identified higher interstory drift in lower and mid-level buildings.

Choinière et al. [35] introduced a simplified linear method, based on Beauchamp, Paultre, and Léger's 2017 proposal, to calculate seismic demands in the gravity load resisting system (GLRS) of shear wall buildings with consideration for foundation movement. The study compared two approaches for modeling foundation movement in linear soil media and evaluated them using nonlinear time history analyses for a 12-story concrete shear wall building.

Noureldin et al. [36] introduced an expert system framework that used supervised machine learning to predict seismic performance in low- to mid-rise structures while considering soil-structure interaction. The framework, which was validated through non-linear time history analysis, incorporated a novel global seismic assessment ratio, resulting in more accurate outcomes compared to traditional methods. It demonstrated high generalization potential, offering comprehensive seismic assessments and design recommendations based on diverse engineering demand parameters.

Sharma et al. [37] employed an artificial neural network (ANN) model to establish a relationship for the effective natural period of reinforced concrete (RC) frame buildings with shear walls and pile foundations in seismic zones. The proposed relationship was shown to be applicable to such structures, offering a more suitable alternative compared to existing relationships designed for shallow foundations.

Requena-Garcia-Cruz et al. [38] investigated the impact of SSI on the seismic vulnerability and losses of a 5-story reinforced concrete (RC) building constructed on soft alluvial strata with shallow foundations. Using nonlinear static analysis (NLSA) and incremental dynamic analysis (IDA) in the OpenSees finite-element framework, the research revealed a significant effect of SSI on the fragility and performance of these structures, with potential worsened damage by up to 38% when considering SSI.

Terzi and Athanatopoulou [39] explored the impact of soil–structure interaction on structural eccentricity in both single-story and multi-story asymmetric buildings, considering the presence of a real elastic axis. The study derived mathematical formulas to determine the coordinates of the elastic axis under flexible base assumptions, highlighting that soil–structure interaction extinguishes the real elastic axis, necessitating the definition

of an optimum torsion axis. Additionally, the research demonstrated that soil–structure interaction reduces structural eccentricity at each story level.

Jesica et al. [40] investigated the impact of SSI on a 10-story reinforced concrete building with a three-level basement during earthquakes in Surabaya, Indonesia. Dynamic time response analyses using nonlinear hysteresis soil springs indicated inconclusive SSI effects, with some scenarios showing increased base shears and inter-story drifts, while others exhibit the opposite results.

Toutanji [41] investigated the effect of foundation rotation on displacements and internal force distribution in shear wall-frame systems under uniform static load.

In a study by Di and Fu [42], the change in displacement and internal force distribution of shear wall-frame systems was explored. This investigation considered the effects of translation and rotation in the foundation under a triangular distributed load.

Both Toutanji and Di and Fu's studies were limited to static analysis, lacking any dynamic analysis components.

Bozdogan et al. [43] investigated the effect of foundation rotation on the dynamic characteristics of buildings featuring various structural systems, including shear walls, frames, and shear wall-frame combinations. The study concluded that foundation rotation increases the displacements but decreases the base shear force. Notably, the study was not examined in analyzing and investigating moment contribution rates.

In summary, the existing literature typically focuses on the impact of foundation rotation on building behavior, and it is usually limited to static uniform or triangular distributed loads. On the contrary, this research investigates the moment distribution at the base, considering the foundation rotation rate, across a total of four distinct loading cases. These cases include parabolic loads and dynamic analysis (first mode), in addition to the previously mentioned loads. Notably, our study incorporates both static and dynamic analyses of moment contribution rates, distinguishing it from Bozdogan et al. [43]. Furthermore, unlike the existing literature, our research accounts for axial displacements in columns and shear walls during analysis. This present study focuses on investigating the impact of foundation rotation on the MCR in shear wall-frame systems. To address this, the wall-frame system is modeled as an equivalent sandwich beam, and practical graphs are generated for various behavior coefficients and rotation ratios. The novelty of the approach proposed in this study lies in the fast and practical determination of the MCR with the presented approach. The presented approach can be particularly useful in the pre-dimensioning stage and for eliminating potential errors in the data entry of detailed analysis software. Although the existing form of the proposed method may not be suitable for analyzing complex buildings, the main emphasis of the study is on offering a rapid and practical solution for preliminary estimates, particularly in the early stages of structural design. From the graphs obtained by the presented method, it is seen that the increase in the foundation rotation results in a decrease in the moment of the shear wall at the base, whereas there is an increase in the frame moment. As a consequence, the predominant structural behavior in systems originally designed as wall-frame configurations tends to shift towards a more frame-centric behavior. In systems of this nature with foundation rotation, the load reduction factor should be redefined, considering this behavioral shift. In the development of the method, it is assumed that the geometry properties are constant throughout the height of the building and that the building is symmetrical in plan.

2. Methods

In this study, the effects of foundation rotation on MCR were examined in detail. Four specific loading scenarios representing wind and earthquake loads were selected for analysis, including uniform static load, triangular distributed load, parabolic distributed load, and dynamic load. Differential equations were derived for each loading case, and the obtained non-homogeneous ordinary differential equations were made dimensionless. Then, dimensionless differential equations were solved by applying boundary conditions, and moment contribution ratios were obtained. The specified boundary conditions include

that the displacement at the base is zero, the bending moment in the base is equal to the product of the spring coefficient of rotation in the foundation and the rotation, and the shear force and moment at the top are zero. The obtained moment contribution ratios were plotted for different structural response coefficients and foundation rotation ratios. For static loading cases, the solution of the differential equations was made analytically, while for the dynamic loading case, the solution was obtained using the differential transformation method [43]. The steps taken in this context are presented as a flow chart in Figure 1.

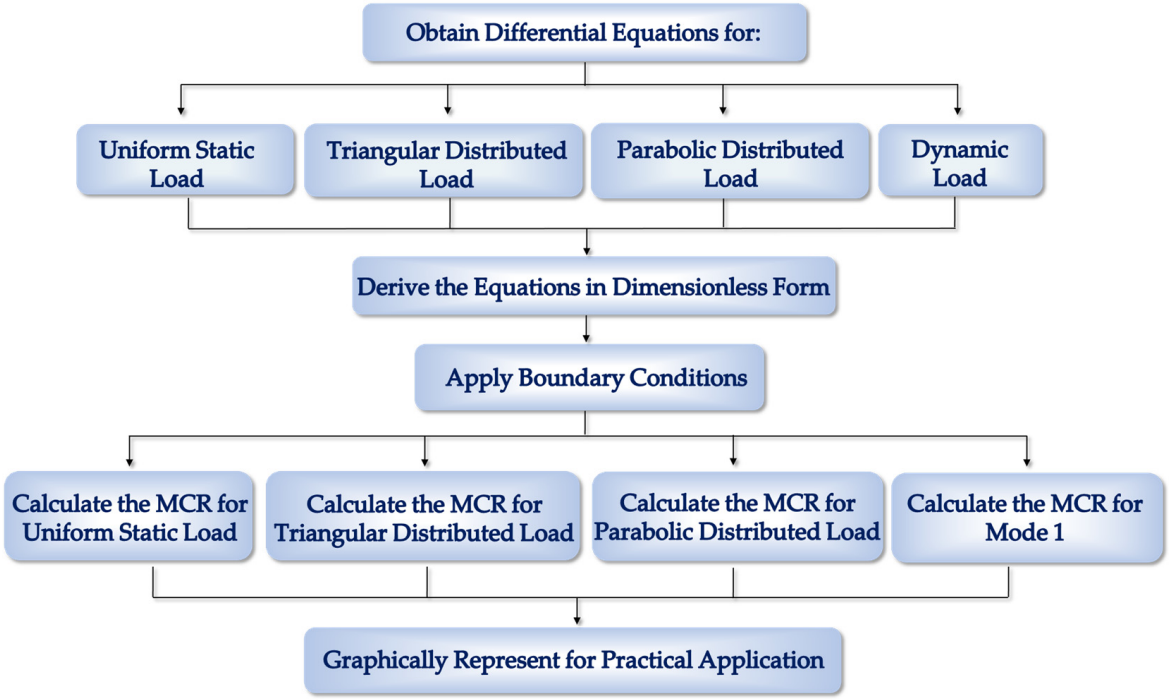

Figure 1. Flowchart illustrating the sequential process steps involved in determining the MCR.

One of the methods used for the analysis of multi-story buildings is the continuum system model. This model is based on the idea of representing multi-story buildings with an equivalent beam to simplify and facilitate the analysis of the behavior of complex multi-story structures [44,45]. The beam models utilized to represent multi-story buildings are the pure flexural beam, the pure shear beam, the Timoshenko beam, and the sandwich beam. In the pure flexural beam model, only the flexural behavior is considered, rendering it particularly suitable for systems with only shear walls. In the pure shear beam model, only the shear behavior is considered, neglecting the flexural behavior, which is more suitable for frame systems where axial displacements can be neglected. The Timoshenko beam model considers both flexural and shear behavior and is particularly suitable for frames where axial deformation is significant. On the other hand, the sandwich beam model fully considers bending, shear, and other deformations in both shear walls and frames. Therefore, in this study, the sandwich beam model is preferred as an equivalent beam model to analyze the behavior of a multi-story reinforced concrete building more effectively. The representation of a multi-story reinforced concrete building as a sandwich beam is shown in Figure 2.

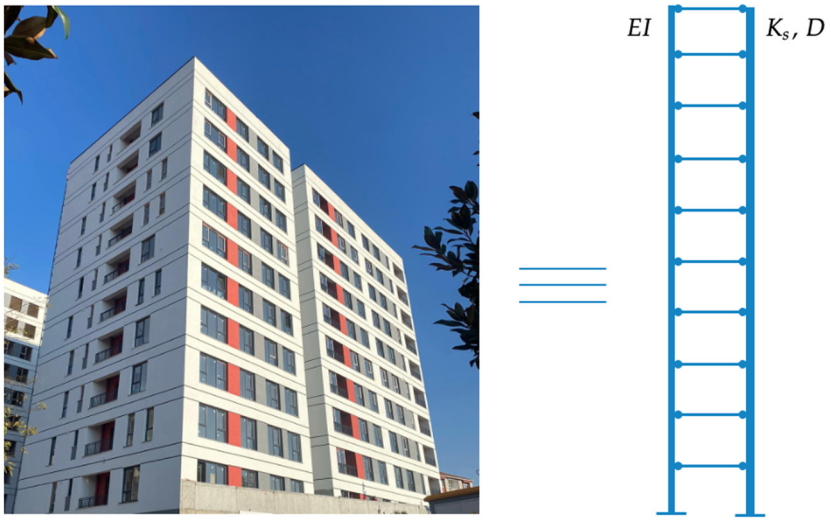

Figure 2. Equivalent sandwich beam model.

2.1. Ordinary Differential Equation for Uniform Static Load

The differential equation representing the behavior under uniform static load can be given as follows:

$$EI\frac{d^4y}{dz^4} - K_s\frac{d^2y}{dz^2} = q_0 \tag{1}$$

Here, EI is the bending stiffness, K_s is the shear stiffness, q_0 is the uniformly distributed load, y is the horizontal displacement function, and z is the vertical axis along the height of the structure. Detailed calculations of the K_s and EI values can be found in Bozdogan et al. [43]. If the following transformation is applied to make Equation (1) dimensionless, the differential equation given by Equation (3) is obtained.

$$\varepsilon = \frac{z}{H} \tag{2}$$

$$\frac{d^4y}{d\varepsilon^4} - \frac{K_s}{EI}H^2\frac{d^2y}{d\varepsilon^2} = \frac{q_0H^4}{EI} \tag{3}$$

In this context, H represents the total height of the building, and ε denotes the dimensionless axis set. Substituting the building behavior coefficient (λ), as defined by Equation (4), into Equation (3) yields Equation (5).

$$\lambda = H\sqrt{\frac{K_s}{EI}} \tag{4}$$

$$\frac{d^4y}{d\varepsilon^4} - \lambda^2\frac{d^2y}{d\varepsilon^2} = A \tag{5}$$

Here, A is defined by Equation (6).

$$A = \frac{q_0H^4}{EI} \tag{6}$$

By solving the differential equation presented in Equation (5), the displacement function seen in Equation (7) is obtained.

$$y(\varepsilon) = c_1 + c_2\varepsilon + c_3cosh(\lambda\varepsilon) + c_4sinh(\lambda\varepsilon) - \frac{A\varepsilon^2}{2\lambda^2} \tag{7}$$

Under these circumstances, the integration constants c_1, c_2, c_3, and c_4 are determined through the application of boundary conditions. The second derivative of the displacement function, which is related to the bending moment function, is obtained as follows with the help of Equation (7).

$$y''(\varepsilon) = c_3\lambda^2 cosh(\lambda\varepsilon) + c_4\lambda^4 sinh(\lambda\varepsilon) - \frac{A}{\lambda^2} \tag{8}$$

2.2. Ordinary Differential Equation for Triangle Static Load

For the case of a triangular distributed load, the differential equation can be written as follows:

$$EI\frac{d^4y}{dz^4} - K_s\frac{d^2y}{dz^2} = \frac{q_0x}{H} \tag{9}$$

Similar to the solution for a uniformly distributed load, making Equation (9) dimensionless yields the following equation.

$$\frac{d^4y}{d\varepsilon^4} - \lambda^2\frac{d^2y}{d\varepsilon^2} = A\varepsilon \tag{10}$$

Upon solving the differential equation represented using Equation (10), Equation (11) yields the displacement function:

$$y(\varepsilon) = c_1 + c_2\varepsilon + c_3 cosh(\lambda\varepsilon) + c_4 sinh(\lambda\varepsilon) - \frac{A\varepsilon^3}{6\lambda^2} \tag{11}$$

To derive the bending moment, Equation (12) is utilized to obtain the expression for the second derivative.

$$y''(\varepsilon) = c_3\lambda^2 cosh(\lambda\varepsilon) + c_4\lambda^2 sinh(\lambda\varepsilon) - \frac{A\varepsilon}{\lambda^2} \tag{12}$$

2.3. Ordinary Differential Equation for Parabolic Static Load

The dimensionless form of the differential equation representing the static equilibrium state for the parabolic loading case is expressed as follows:

$$\frac{d^4y}{d\varepsilon^4} - \lambda^2\frac{d^2y}{d\varepsilon^2} = A\varepsilon^2 \tag{13}$$

By solving Equation (13), the displacement function for the parabolic distributed load case is obtained as follows:

$$y(\varepsilon) = c_1 + c_2\varepsilon + c_3 cosh(\lambda\varepsilon) + c_4 sinh(\lambda\varepsilon) - \frac{A\varepsilon^4}{12\lambda^2} - \frac{A\varepsilon^2}{\lambda^4} \tag{14}$$

The second derivative function related to the bending moment function, Equation (15), is obtained using the displacement function given in Equation (14).

$$y''(\varepsilon) = c_3\lambda^2 cosh(\lambda\varepsilon) + c_4\lambda^2 sinh(\lambda\varepsilon) - \frac{A\varepsilon^2}{\lambda^2} - \frac{2A}{\lambda^4} \tag{15}$$

2.4. Ordinary Differential Equation for Dynamic Load

In the case of free vibration, the differential equation can be written as follows:

$$EI\frac{d^4y}{dz^4} - K_s\frac{d^2y}{dz^2} - \overline{m}\omega^2 y = 0 \tag{16}$$

The differential equation presented above was previously solved in the literature using the differential transformation method (Bozdogan et al. [43]). Therefore, without

discussing the properties of the solution here, the shear wall moment contribution rate was determined using the mode shape function found in the existing literature.

2.5. Boundary Conditions

Obtaining integration constants in the differential equation requires establishing common boundary conditions for uniform distributed load, triangular distributed load, parabolic distributed load, and dynamic load. These shared conditions encompass:

1. Displacement at the base equals zero:

$$\varepsilon = 0 \quad or \quad y = 0 \tag{17}$$

2. The bending moment in the base is equal to the product of the spring coefficient of rotation in the foundation and the rotation:

$$\frac{EI}{H^2}\frac{d^2y}{d\varepsilon^2} = \frac{kr}{H}\frac{dy}{d\varepsilon} \tag{18}$$

$$\frac{EI}{Hkr}\frac{d^2y}{d\varepsilon^2} = \frac{dy}{d\varepsilon} \tag{19}$$

$$\rho\frac{d^2y}{d\varepsilon^2} = \frac{dy}{d\varepsilon} \tag{20}$$

$$\rho = \frac{EI}{Hkr} \tag{21}$$

where ρ is the rotation ratio.

3. Zero bending moment at the top:

$$\frac{EI}{H^2}\frac{d^2y}{d\varepsilon^2}\bigg|_{\varepsilon=1} = 0 \tag{22}$$

4. Zero shear force at the top:

$$\frac{d^3y}{d\varepsilon^3} - \lambda^2\frac{dy}{d\varepsilon} = 0 \tag{23}$$

3. Variation of Moment Contribution Ratio

The MCR variation concerning the structural behavior coefficient is explored for different foundation rotation ratios across various loading scenarios. These scenarios encompass static uniform, triangular, and parabolic loads, along with dynamic analysis (first mode).

3.1. Moment Contribution Ratio for Uniform Static Load

In this section, MCR values are determined for different rotation ratios in shear wall frame systems under uniform distributed load. Figure 3 depicts a shear wall frame subjected to a uniform distributed load.

For a uniformly distributed load, the following equation can be written for the MCR (α_m), representing the ratio of the moment taken by the shear wall at the base to the total overturning moment.

$$\alpha_m = \frac{\frac{d^2y}{d\varepsilon^2}\Big|_{\varepsilon=0}}{\frac{qH^4}{2EI}} = \frac{2\frac{d^2y}{d\varepsilon^2}\Big|_{\varepsilon=0}}{A} \tag{24}$$

Substituting $\varepsilon = 0$ in Equation (8) and replacing α_m above becomes the following equation:

$$\alpha_m = 2\frac{c_3\lambda^2 - \frac{A}{\lambda^2}}{A} \tag{25}$$

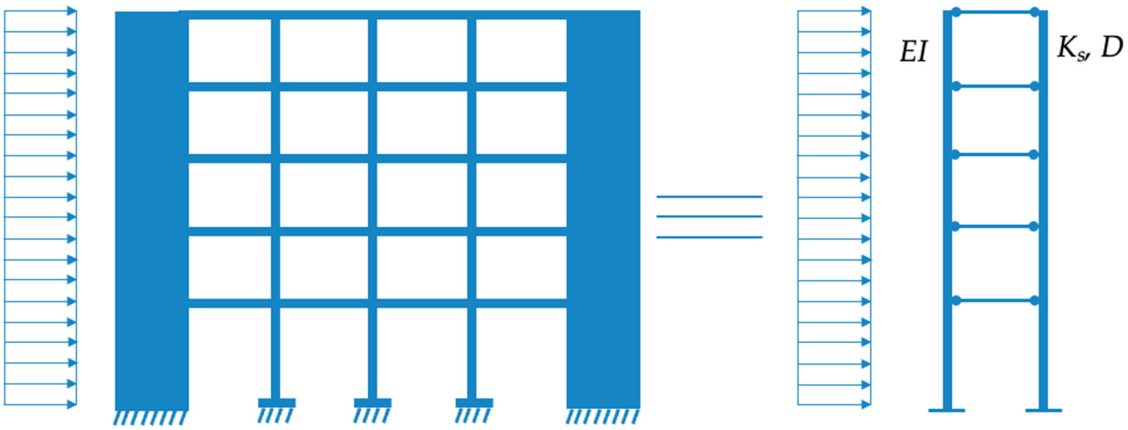

Figure 3. Shear wall-frame under uniform distributed load.

Utilizing the horizontal displacement function provided in Equation (7) and considering the boundary conditions, c_3 is obtained as follows.

$$c_3 = \frac{\frac{A}{\lambda^2}[1 + (1+\rho)\lambda sinh(\lambda)]}{[\lambda^3\rho sinh(\lambda) + \lambda^2 cosh(\lambda)]} \tag{26}$$

Upon substituting the value of c_3 into Equation (26), the coefficient αm is determined as follows:

$$\alpha_m = 2\left\{\frac{[1 + (1+\rho)\lambda sinh(\lambda)]}{\lambda^3\rho sinh(\lambda) + \lambda^2 cosh(\lambda)} - \frac{1}{\lambda^2}\right\} \tag{27}$$

Using the above relation, the MCR (α_m) has been calculated for different foundation rotation ratios (ρ) and various structural behavior coefficients (λ), as illustrated in Figure 4. In this context, $\lambda = 0$ represents the shear wall case, while $\lambda = 20$ represents the frame case, and ρ-values indicate the foundation rotation; for example, $\rho = 0$ signifies no foundation rotation. This graph enables the determination of the MCR (α_m) value based on λ and ρ-values.

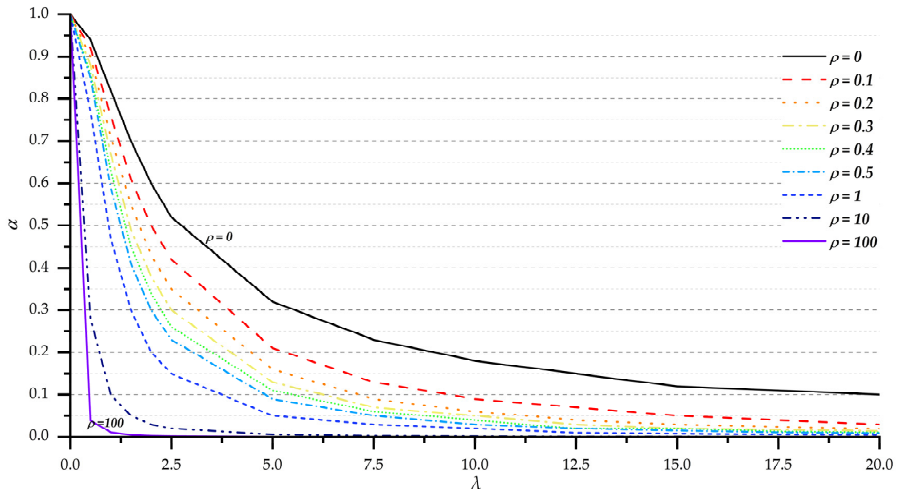

Figure 4. Variation of moment contribution ratio depending on structural behavior coefficient and foundation rotation ratio for uniformly distributed load.

As depicted in Figure 4, there is a decrease in the MCR with an increase in the foundation rotation ratio under static uniform load conditions.

3.2. Moment Contribution Ratio for Triangle Static Load

This section investigates the determination of MCR values for various rotation ratios within shear wall-frame systems, specifically under the influence of a triangular distributed load. The configuration of a shear wall-frame subjected to this load is visually represented in Figure 5.

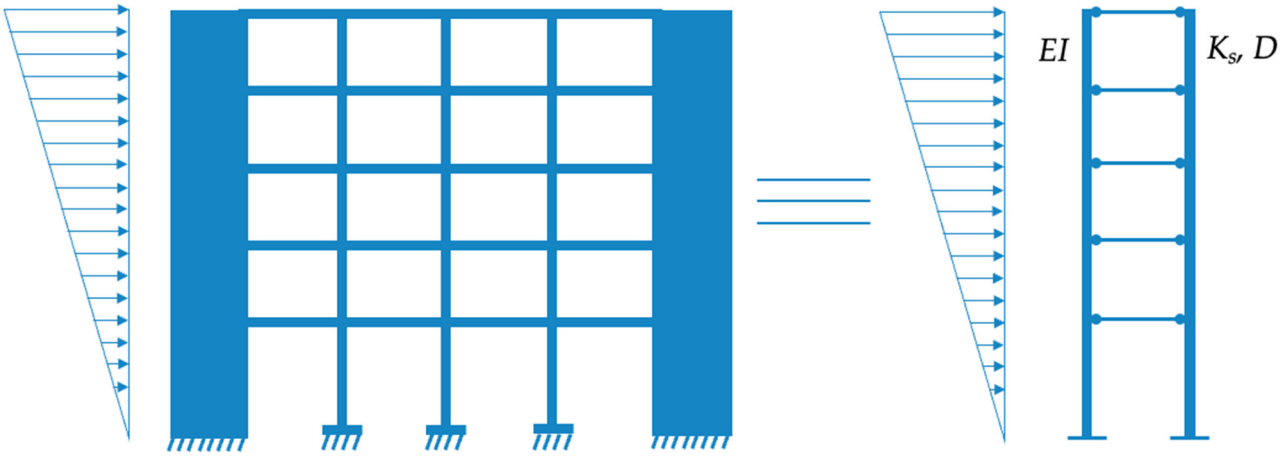

Figure 5. Shear wall-frame under triangle distributed load.

In the case of a triangular distributed load, the MCR (α_m) is written as follows:

$$\alpha_m = \frac{\frac{EI}{H^2}\frac{d^2y}{d\varepsilon^2}\Big|_{\varepsilon=0}}{\frac{qH^2}{3}} \tag{28}$$

Upon making the required simplifications in Equation (28), Equation (29) is obtained:

$$\alpha_m = \frac{\frac{d^2y}{d\varepsilon^2}\Big|_{\varepsilon=0}}{\frac{qH^4}{3EI}} = \frac{3\frac{d^2y}{d\varepsilon^2}\Big|_{\varepsilon=0}}{A} \tag{29}$$

Substituting $\varepsilon = 0$ into Equation (12) and placing it in Equation (29) yields Equation (30).

$$\alpha_m = 3\frac{c_3\lambda^2}{A} \tag{30}$$

Using Equation (11) and applying the boundary conditions, the value of c_3 is determined as follows:

$$c_3 = \frac{\frac{A}{\lambda^2}\left[1 + \left(\frac{1}{2} - \frac{1}{\lambda^2}\right)\lambda sinh(\lambda)\right]}{[\rho\lambda^3 sinh(\lambda) + \lambda^2 cosh(\lambda)]} \tag{31}$$

Substituting the obtained value of c_3 from Equation (31) into Equation (30) yields the coefficient α_m for the triangular distributed load case, as follows.

$$\lambda_3 = 3\left\{\frac{\left[1 + \left(\frac{1}{2} - \frac{1}{\lambda^2}\right)\lambda sinh(\lambda)\right]}{[\rho\lambda^3 sinh(h) + \lambda^2 cosh(\lambda)]}\right\} \tag{32}$$

Equation (32) is utilized to calculate αm values for different foundation rotation ratios (ρ) and various structural behavior coefficients (λ). The graphical representation of these results is presented in Figure 6.

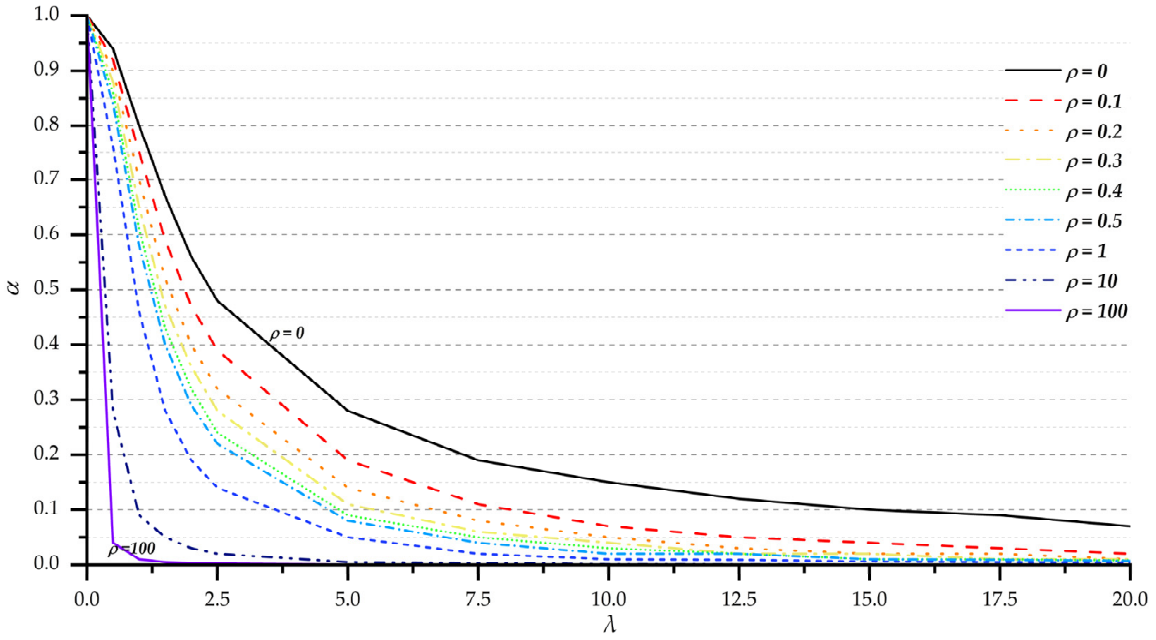

Figure 6. Variation of moment contribution ratio depending on structural behavior coefficient and foundation rotation ratio for triangular distributed load.

3.3. Moment Contribution Ratio for Parabolic Static Load

In this section, the determination of MCR values is investigated for various rotation ratios within shear wall-frame systems, particularly under the influence of a parabolic distributed load. The configuration of a shear wall-frame subjected to this load is visually represented in Figure 7.

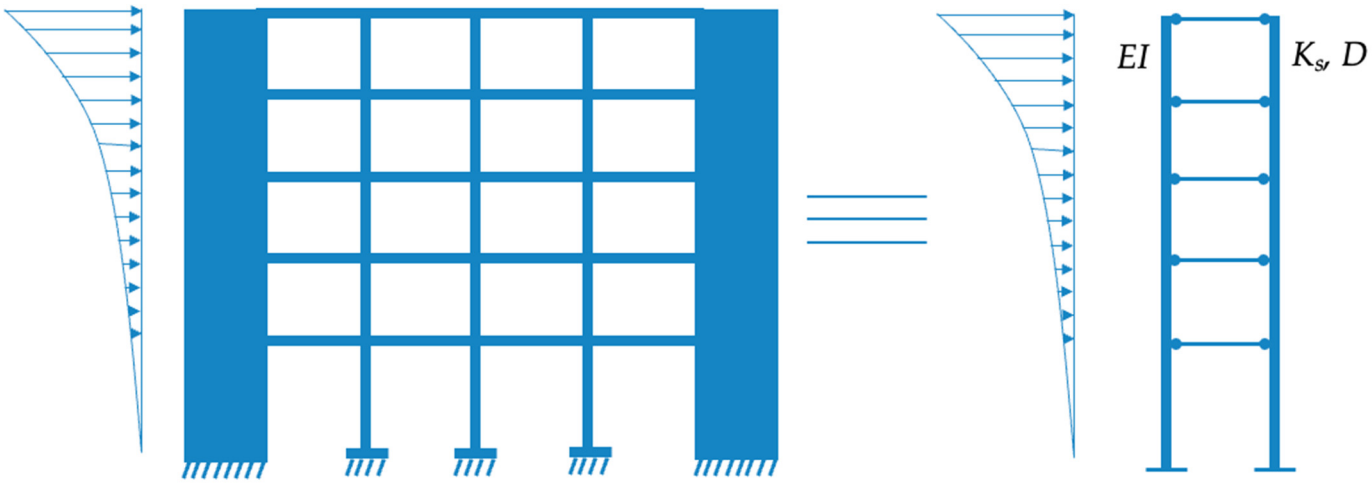

Figure 7. Shear wall-frame under parabolic distributed load.

For the parabolic loading case, the α_m relation is given as follows:

$$\alpha_m = \frac{\frac{EI}{H^2}\frac{d^2y}{d\varepsilon^2}\Big|_{\varepsilon=0}}{\frac{qH^2}{4}} \quad (33)$$

Equation (33) can be written as follows:

$$\alpha_m = \frac{\frac{d^2y}{d\varepsilon^2}\Big|_{\varepsilon=0}}{\frac{qH^4}{4EI}} = \frac{4\frac{d^2y}{d\varepsilon^2}\Big|_{\varepsilon=0}}{A} \tag{34}$$

Written as $\varepsilon = 0$ in Equation (15) and substituted into Equation (34), the expression for α_m is as follows:

$$\alpha_m = 4\frac{c_3\lambda^2 - \frac{2A}{\lambda^4}}{A} \tag{35}$$

Using the displacement function given by Equation (14) and the boundary conditions for the parabolic loading case, c_3 is obtained as follows:

$$c_3 = \frac{\frac{A}{3\lambda^2}sinh(\lambda) + \frac{A}{\lambda^2} + \frac{2A}{\lambda^4}}{[\rho\lambda^3 sinh(\lambda) + \lambda^2 cosh(\lambda)]} - \frac{2A}{\lambda^4} \tag{36}$$

By substituting Equation (36) in Equation (35), the α_m ratio for the parabolic loading case is obtained as follows:

$$\alpha_m = 4\left\{\frac{\frac{1}{3}\lambda sinh(\lambda) + 1 + \frac{2}{\lambda^2}}{\rho\lambda^3 sinh(\lambda) + \lambda^2 cosh(\lambda)} - \frac{2}{\lambda^4}\right\} \tag{37}$$

The α_m values obtained with Equation (37) are calculated for various foundation rotation ratios (ρ) and different structural behavior coefficient (λ) values, and they are presented graphically in Figure 8.

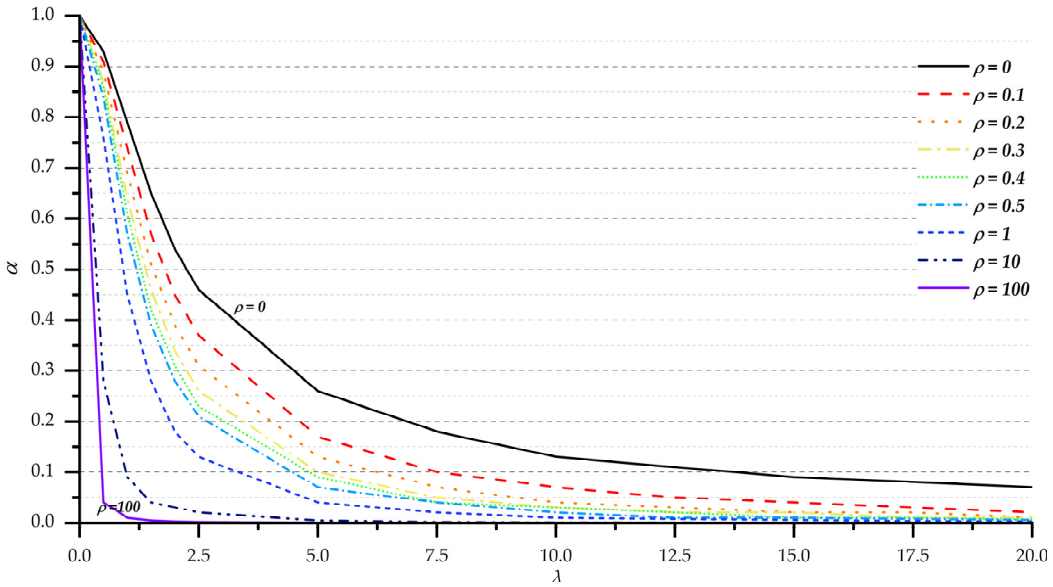

Figure 8. Variation of moment contribution ratio depending on structural behavior coefficient and foundation rotation ratio for parabolic distributed load.

3.4. Moment Contribution Ratio for Dynamic Load

In the case of dynamic analysis, Mode 1 is considered to determine the MCR. The solution of Equation (16) using the differential transformation method given in the literature by [43], the MCR value is calculated using Equation (38) for Mode 1.

$$\alpha_m = \frac{\Gamma_1 \frac{EI}{H^2}\frac{d^2y}{dz^2}\Big|_{\varepsilon=0} S_{d1}}{eko_1 M_t\, Sa(T_1) v_1 H} \tag{38}$$

where Γ_1 is the modal participation factor of the first mode, S_{d1} is the spectral displacement in the first mode, eko_1 is the effective mass ratio of the first mode, y'' is the second derivative of the first mode shape, M_t is the total building mass, $Sa(T_1)$ is the spectral acceleration corresponding to the first mode, and υ_1 is the ratio of the effective height of the first mode to the total building height (H). As known from the basic concepts of structural dynamics, the effective height (H^*) is defined as the height from the base to the center of mass of the first mode.

$$H^* = \upsilon_1 H \tag{39}$$

Here υ_1 is found by the following relation:

$$\upsilon_1 = \frac{\sum_j^n (m_j y_{j1} \varepsilon_j)}{\sum_j^n (m_j {y_{j1}}^2)} \tag{40}$$

For Mode 1, the period value is calculated using the following Equation from [43]:

$$T_1 = S_1 H^2 \sqrt{\frac{\overline{m}}{EI}} \tag{41}$$

In the above relationship, the distributed mass ($\overline{m}$) can be written as the ratio of the total building mass to the building height as in Equation (42).

$$T_1 = S_1 H^2 \sqrt{\frac{M_t}{HEI}} \tag{42}$$

Hence, the equivalent of EI/H^2 is obtained as follows.

$$\frac{EI}{H^2} = {S_1}^2 \frac{M_t H}{{T_1}^2} \tag{43}$$

By substituting this expression in Equation (38), the MCR is obtained as follows:

$$\alpha_m = \frac{\Gamma_1 \, {S_1}^2 \frac{M_t H}{{T_1}^2} \left.\frac{d^2 y}{dz^2}\right|_{\varepsilon=0} S_{d1}}{eko_1 \; M_t \; Sa(T_1) \quad \upsilon_1 \; H} \tag{44}$$

Using the relation given in Equation (45) instead of the period yields Equation (46).

$$T_1 = \frac{2\pi}{\omega} \tag{45}$$

$$\alpha_m = \frac{\Gamma_1 \, {S_1}^2 \frac{M_t H}{4\pi^2} \left.\frac{d^2 y}{dz^2}\right|_{\varepsilon=0} \omega_1^2 \, S_{d1}}{eko_1 \; M_t \; Sa(T_1) \quad \upsilon_1 \; H} \tag{46}$$

Equation (48) is derived by utilizing the relationship between spectral acceleration and spectral displacement, as known from structural dynamics and presented in Equation (47).

$$Sa(T_1) = \omega_1^2 * S_{d1} \tag{47}$$

$$\alpha_m = \frac{\Gamma_1 \, {S_1}^2 \frac{1}{4\pi^2} \left.\frac{d^2 y}{dz^2}\right|_{\varepsilon=0}}{eko_1 \; \upsilon_1} \tag{48}$$

Replacing the second derivative of the first mode given in Equation (48) with the transformation function obtained from the differential transformation method detailed in the literature, Equation (49) is derived.

$$\alpha_m = \frac{\Gamma_1 \, {S_1}^2 \frac{1}{4\pi^2} 2 \, Y[2]}{eko_1 \, v_1} \tag{49}$$

By making the required adjustments in the given equation, the MCR can be determined using the following relationship:

$$\alpha_m = \frac{\Gamma_1 \, {S_1}^2 \frac{1}{2\pi^2} Y[2]}{eko_1 \, v_1} \tag{50}$$

MCR values for different rotation ratios and different structural behavior coefficient values are calculated using the above relation and shown in Figure 9.

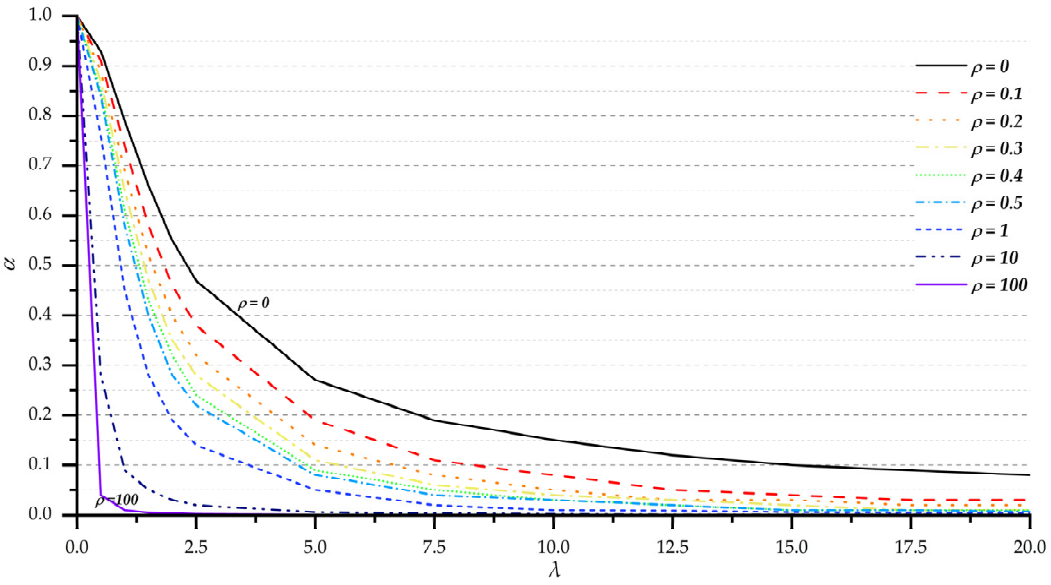

Figure 9. Variation of moment contribution ratio depending on structural behavior coefficient and foundation rotation ratio for dynamic load (Mode 1).

4. Validation of the Proposed Method with Finite Element Method

4.1. Example 1

In this section, to illustrate the effectiveness of the method proposed in this study, we solved three different systems depicted in Figure 10 (System 1, System 2, and System 3). In System 1, where λ = 0.987, since the shear wall dimensions are large, the shear wall is more dominant in the behavior. In System 2, where λ = 2.740, since the ratio of shear walls and frame is balanced, the behavior is seen as a combination of shear walls and frame. In System 3, where λ = 9.490, since the ratio of shear walls is low, the behavior is more dominated by the frame.

In the example, the modulus of elasticity is 3×10^7 kN/m^2, the columns are 35 cm/35 cm in size, and the beams are 25 cm/40 cm in size (T beam). The shear wall is 50 cm/500 cm in System 1, 30 cm/300 cm in System 2, and 20 cm/150 cm in System 3. It is assumed that the sections are cracked sections. For this, the moment of inertia of the columns is multiplied by 0.7, the moment of inertia of the beams by 0.35, and the moment of inertia of the shear wall by 0.5 coefficient. The parameters required for the analysis using the proposed method presented in this study are given in Table 1 for Systems 1, 2, and 3.

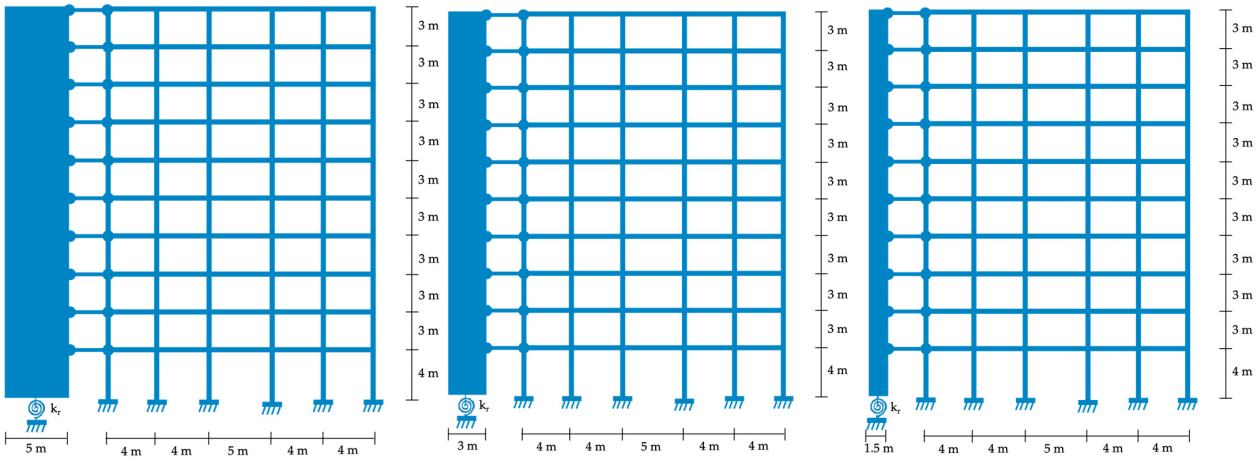

(**a**) (**b**) (**c**)

Figure 10. Structural systems used for validation: (**a**) System 1, (**b**) System 2, and (**c**) System 3.

Table 1. Parameters used in the examples.

	System 1	System 2	System 3
K_S (kN)	80,149.99	80,149.99	80,149.99
EI (kN·m^2)	78,125,000	10,125,000	843,750
D (kN·m^2)	1,166,812,500	1,166,812,500	1,166,812,500
K_{Se} (kN)	79,102.51	79,102.51	79,102.51
λ	0.987	2.740	9.490

The MCR analysis is performed for three distinct systems using the SAP2000 Software (Version 22), considering five distinct rotation ratios: $\rho = 0$, $\rho = 0.1$, $\rho = 0.3$, $\rho = 0.5$, and $\rho = 1$. The obtained results are then compared with those derived from the approach proposed in this study and tabulated in Tables 2–4 for Systems 1, 2, and 3, respectively. The comparison is conducted for four different load cases: spectral analysis (dynamic), uniform distributed load, triangular distributed load, and parabolic distributed load.

Table 2. Variation of MCR values for System 1.

Wall-Frame (System 1)								
	Spectral Analysis		Uniform Distributed Load		Triangular Distributed Load		Parabolic Distributed Load	
	Proposed Method	SAP2000	Proposed Method	SAP2000	Proposed Method	SAP2000	Proposed Method	SAP2000
$\rho = 0$	0.79	0.80	0.82	0.83	0.80	0.83	0.79	0.80
$\rho = 0.1$	0.74	0.75	0.76	0.77	0.75	0.77	0.74	0.75
$\rho = 0.3$	0.66	0.66	0.68	0.68	0.66	0.68	0.65	0.66
$\rho = 0.5$	0.59	0.59	0.60	0.61	0.60	0.61	0.58	0.59
$\rho = 1$	0.46	0.47	0.48	0.48	0.47	0.48	0.46	0.47

Table 3. Variation of MCR values for System 2.

Wall-Frame (System 2)								
	Spectral Analysis		Uniform Distributed Load		Triangular Distributed Load		Parabolic Distributed Load	
	Proposed Method	SAP2000	Proposed Method	SAP2000	Proposed Method	SAP2000	Proposed Method	SAP2000
$\rho = 0$	0.45	0.44	0.50	0.50	0.46	0.45	0.44	0.43
$\rho = 0.1$	0.36	0.35	0.40	0.43	0.37	0.36	0.35	0.34
$\rho = 0.3$	0.26	0.25	0.28	0.30	0.26	0.25	0.26	0.24
$\rho = 0.5$	0.21	0.19	0.22	0.24	0.21	0.19	0.20	0.18
$\rho = 1$	0.13	0.12	0.14	0.15	0.13	0.12	0.12	0.12

Table 4. Variation of MCR values for System 3.

	Wall-Frame (System 3)							
	Spectral Analysis		**Uniform Distributed Load**		**Triangular Distributed Load**		**Parabolic Distributed Load**	
	Proposed Method	**SAP 2000**	**Proposed Method**	**SAP 2000**	**Proposed Method**	**SAP 2000**	**Proposed Method**	**SAP 2000**
$\rho = 0$	0.16	0.15	0.19	0.19	0.16	0.14	0.14	0.13
$\rho = 0.1$	0.09	0.08	0.10	0.10	0.08	0.08	0.08	0.07
$\rho = 0.3$	0.04	0.04	0.05	0.05	0.04	0.04	0.034	0.036
$\rho = 0.5$	0.03	0.03	0.03	0.03	0.02	0.03	0.024	0.024
$\rho = 1$	0.01	0.02	0.022	0.019	0.012	0.015	0.012	0.013

As seen from the tables, the results obtained from this study are consistent with the results of SAP 2000, employing finite element analysis methods.

In the study, the effect of a single mode is considered in calculating MCR values in the spectral analysis (dynamic), assuming that the contribution of higher modes is negligible. To demonstrate the validity of this assumption, MCR values were calculated by considering all ten modes in the SAP2000 analysis for the three systems in question. These values were then compared with the MCR values obtained for a single mode, as presented in Table 5. The results of the analysis in Table 5 clearly show that the consideration of a single mode is sufficient.

Table 5. Comparison of MCR values obtained with SAP2000 for single mode and ten modes.

	Spectral Analysis (λ = 0.987)		**Spectral Analysis (λ = 2.740)**		**Spectral Analysis (λ = 9.490)**	
	Single Mode	**Ten Mode**	**Single Mode**	**Ten Mode**	**Single Mode**	**Ten Mode**
$\rho = 0$	0.80	0.82	0.44	0.48	0.15	0.16
$\rho = 0.1$	0.75	0.76	0.35	0.37	0.08	0.08
$\rho = 0.3$	0.66	0.67	0.25	0.26	0.04	0.04
$\rho = 0.5$	0.59	0.60	0.19	0.20	0.03	0.03
$\rho = 1$	0.47	0.47	0.12	0.13	0.02	0.02

4.2. Example 2

MCR values of an eight-story building, taken from the literature [46] and whose floor plan is shown in Figure 11, were calculated using the method proposed in this study, and the results obtained were compared with both literature [46] data and SAP2000.

In this example, the modulus of elasticity is 3×10^7 kN/m^2, the story height is 3.5 m, and the columns are 60 cm/60 cm in size, while the beams are 25 cm/50 cm. The shear walls have dimensions of 20 cm by 500 cm. Table 6 provides the necessary parameters for the analysis using the proposed method outlined in this study. The MCR analysis is conducted using the SAP2000 software, considering five distinct rotation ratios ($\rho = 0$, $\rho = 0.1$, $\rho = 0.3$, $\rho = 0.5$, and $\rho = 1$). Results obtained from this analysis were compared with those derived from the method proposed in this study and are tabulated in Table 7. The comparison is performed for two different load cases: spectral analysis and triangular distributed load.

Within the scope of this study, in order to investigate whether it is sufficient to consider a single mode in dynamic analysis, analyses are performed in SAP2000 with a single mode and eight modes, and the results are given in Table 8. As can be seen from the table, since the single-mode and eight-mode results are identical, it is clearly seen that it is sufficient to perform the analysis considering single mode.

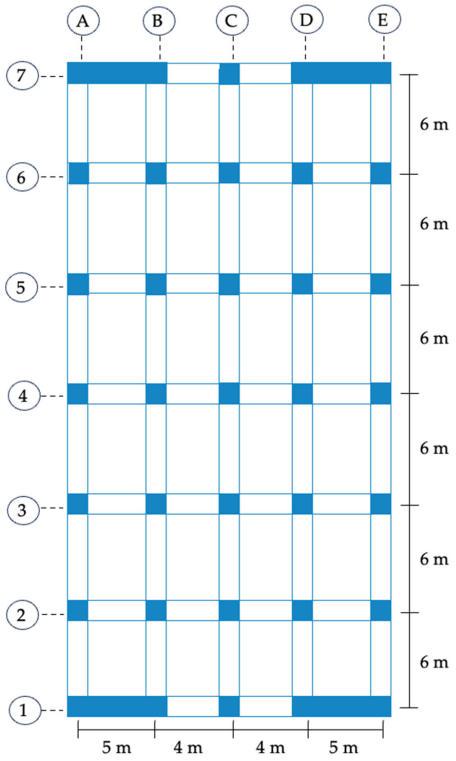

Figure 11. Storey plan for Example 2.

Table 6. Parameters used in Example 2.

	Example 2
K_S (kN)	1,735,805.524
EI (kN·m^2)	250,000,000
D (kN·m^2)	1.5546×10^{10}
K_{Se} (kN)	1,705,985.398
λ	2.31

Table 7. Comparison of MCR values for Example 2.

	Spectral Analysis			**Triangular Distributed Load**		
	Proposed Method	**SAP2000**	**[46]**	**Proposed Method**	**SAP2000**	**[46]**
$\rho = 0$	0.50	0.51	0.44	0.51	0.51	0.49
$\rho = 0.1$	0.41	0.40	-	0.42	0.40	-
$\rho = 0.3$	0.31	0.32	-	0.31	0.32	-
$\rho = 0.5$	0.24	0.27	-	0.25	0.27	-
$\rho = 1$	0.16	0.19	-	0.16	0.19	-

Table 8. Comparison of the MCR values obtained with SAP 2000 for single and eight modes.

	Spectral Analysis	
	Single Mode	**Eight Mode**
$\rho = 0$	0.51	0.51
$\rho = 0.1$	0.40	0.43
$\rho = 0.3$	0.32	0.32
$\rho = 0.5$	0.27	0.27
$\rho = 1$	0.19	0.19

4.3. Example 3

In this example, the building selected from the literature [47], whose plan is shown in Figure 12, is analyzed as 8-story and 15-story. The results obtained are then compared with the results obtained from the literature and SAP2000. In the example, columns are 50 cm/50 cm in the 8-story building, 60 cm/60 cm in the 15-story building; beams are 25 cm/50 cm, and shear walls are 30 cm/525 cm and 30 cm/425 cm. The modulus of elasticity is 3.18×10^6 kN/m^2, and the story height is 3 m. Table 9 shows the parameters required for the analysis with the method proposed in this study. MCR values were carried out using the SAP2000 program considering five different rotation ratios: $\rho = 0$, $\rho = 0.1$, $\rho = 0.3$, $\rho = 0.5$, and $\rho = 1$. The results obtained are then compared with the results obtained from the approach proposed in this study and are given in Tables 10 and 11 for 8-story and 15-story buildings, respectively. The comparison is carried out for two different load cases: spectral analysis and triangular distributed load. In the given example, the MCR values were calculated manually for the x direction.

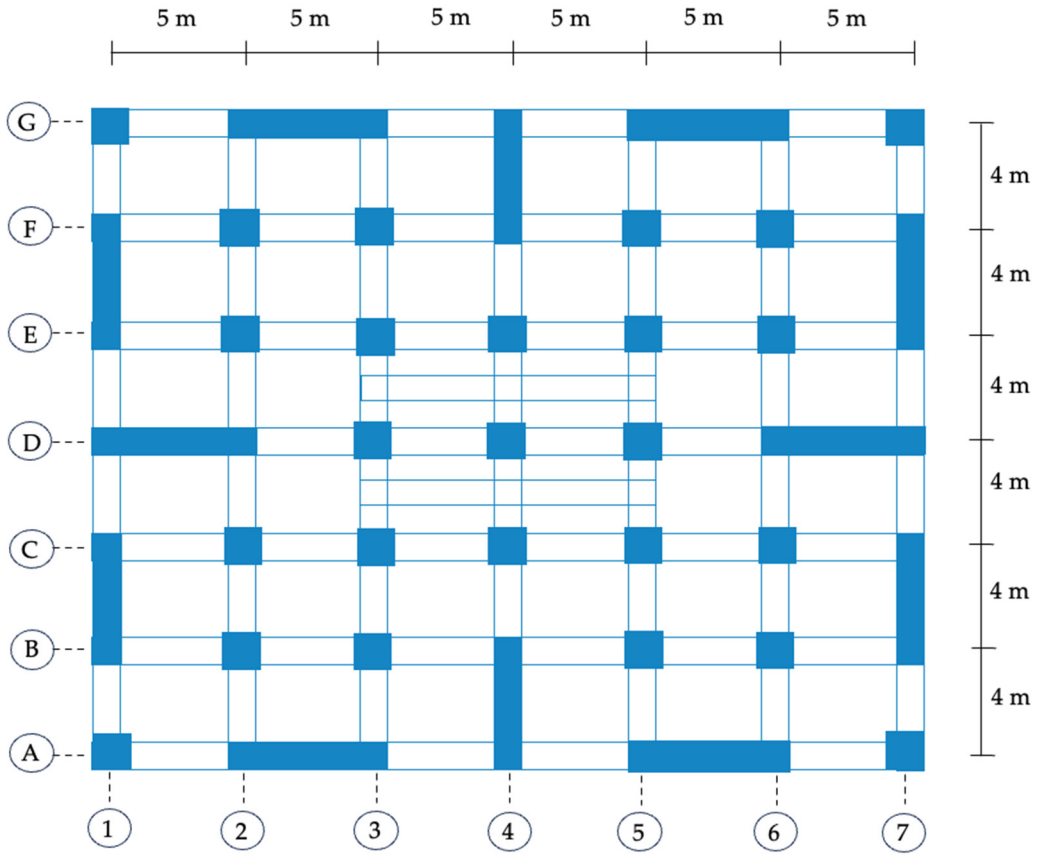

Figure 12. Story plan for Example 3.

Table 9. Parameters used in Example 3.

	8-Story	**15-Story**
K_S (kN)	2,646,995.748	2,843,021.552
EI (kN·m^2)	676.89×10^6	676.89×10^6
D (kN·m^2)	4277.20×10^6	4277.20×10^6
K_{Se} (kN)	2,633,727.517	2,772,541.44
λ	1.5	2.88

Table 10. Comparison of MCR values for Example 3 (8-Storey).

	Spectral Analysis		Triangular Distributed Load		
	Proposed Method	**SAP2000**	**Proposed Method**	**SAP2000**	**[47]**
$\rho = 0$	0.66	0.64	0.67	0.64	0.64
$\rho = 0.1$	0.58	0.49	0.59	0.49	-
$\rho = 0.3$	0.47	0.41	0.47	0.41	-
$\rho = 0.5$	0.40	0.35	0.40	0.35	-
$\rho = 1$	0.28	0.26	0.28	0.26	-

Table 11. Comparison of MCR values for Example 3 (15-story).

	Spectral Analysis		Triangular Distributed Load		
	Proposed Method	**SAP2000**	**Proposed Method**	**SAP2000**	**[47]**
$\rho = 0$	0.44	0.43	0.45	0.42	0.45
$\rho = 0.1$	0.35	0.31	0.36	0.31	
$\rho = 0.3$	0.25	0.22	0.25	0.22	
$\rho = 0.5$	0.20	0.17	0.20	0.17	
$\rho = 1$	0.13	0.11	0.13	0.11	

In this example, in order to investigate whether a single mode is sufficient for dynamic analysis, single-mode and multi-mode analyses are performed in SAP2000, and the results are shown in Table 12. The results are presented in Table 11, indicating that single-mode analysis is sufficient for determining MCR values.

Table 12. Comparison of MCR values obtained with SAP 2000 for single mode and multi-mode.

	8-Story		15-Story	
	Single Mode	**Eight Mode**	**Single Mode**	**Fifteen Mode**
$\rho = 0$	0.64	0.64	0.42	0.43
$\rho = 0.1$	0.49	0.49	0.31	0.31
$\rho = 0.3$	0.41	0.41	0.22	0.22
$\rho = 0.5$	0.35	0.35	0.17	0.17
$\rho = 1$	0.26	0.26	0.11	0.11

5. Results

The graphs illustrated in Figures 4, 6, 8, and 9 clearly show that there is a decrease in the MCR as the foundation rotation rate increases. Moreover, this decrease is evident for higher structural behavior coefficients. In particular, the changes in moment contribution ratios are quite consistent for dynamic (first mode), triangular, and parabolic load distributions. However, a slightly higher variation is observed in the case of a uniformly distributed load. The rotations under the shear walls cause the loads acting on the shear walls to be transferred to the frames. As a result, the frames are subjected to unexpected stresses that are initially ignored, as illustrated in Figure 13.

Although no exact moment contribution ratio value defines the boundaries of pure shear wall and pure frame behavior, this study considers the ranges of shear wall and frame behavior for two different boundary values. These two different limits are the limit states used in the revision of the load-reduction coefficient in seismic codes.

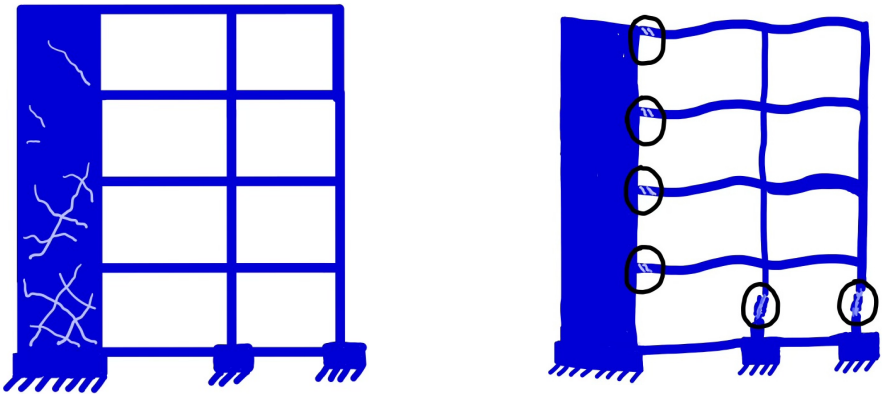

(**a**) (**b**)

Figure 13. Effect of foundation rotation on load distribution in shear wall-frame structures: (**a**) under no foundation rotation, and (**b**) with foundation rotation.

In the first assumption, it is assumed that if the shear wall moment contribution ratio is greater than 0.75, pure shear wall behavior is exhibited, and if it is less than 0.40, pure frame behavior is exhibited. The change in the structural behavior coefficient for pure shear wall, pure frame, and shear wall-frame behavior depending on the foundation rotation is examined and shown in Figure 14. In the absence of foundation rotation ($\rho = 0$), the building predominantly displays pure shear wall behavior for structural behavior coefficient values below 1.15, diminishing rapidly with increasing ρ. For instance, at $\rho = 0.2$, this threshold decreases to 0.85 and further reduces to 0.66 at $\rho = 0.5$. The upper limit value denoting pure frame behavior is 3.1 at $\rho = 0$, but it diminishes to 2 at $\rho = 0.2$ and 1.5 at $\rho = 0.5$.

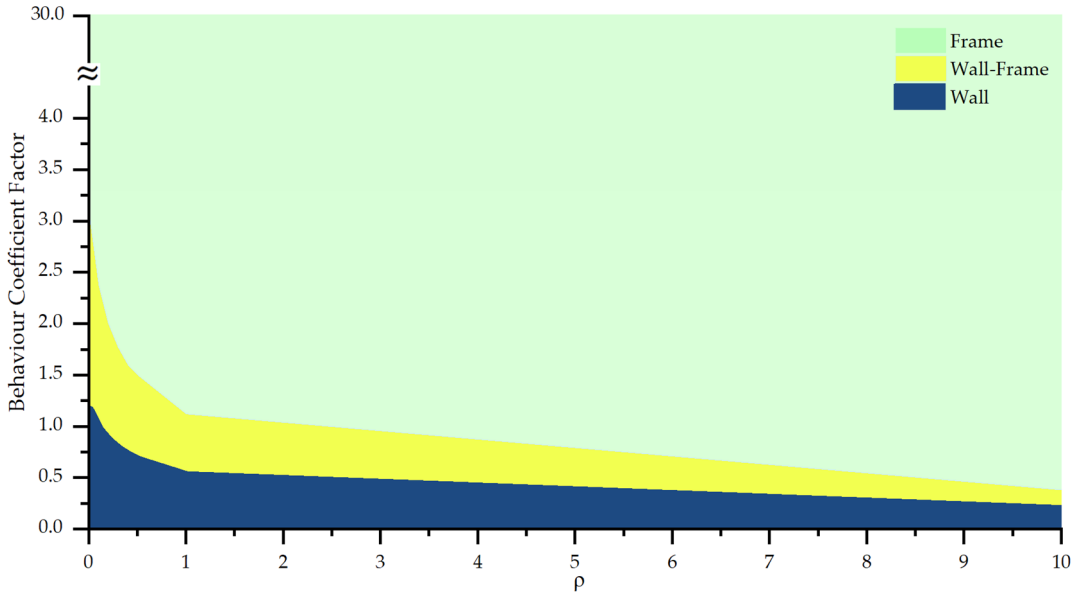

Figure 14. Variation of the structural behavior based on the MCR (assumption 1).

In the second assumption, for shear wall and frame behavior, it is accepted that for values of shear wall MCR less than 0.66, the behavior is pure shear wall behavior, whereas for values less than 0.33, the behavior is pure frame behavior. Similar to the first assumption, for the second assumption, the change in the structural behavior coefficient depending on the limits of shear wall, frame, and shear wall-frame system behavior for different MCRs is shown in Figure 15. As can be seen from Figure 15, in the absence of foundation rotation, values of the structural behavior coefficient less than 1.5 indicate pure shear wall behavior, while this ratio decreases to 1.09 for $\rho = 0.2$ and 0.83 for $\rho = 0.5$. On the other hand, while

the limit for pure frame behavior is 4 for $\rho = 0$, i.e., no foundation rotation, it becomes 2.45 for $\rho = 0.2$ and 1.75 for $\rho = 0.5$.

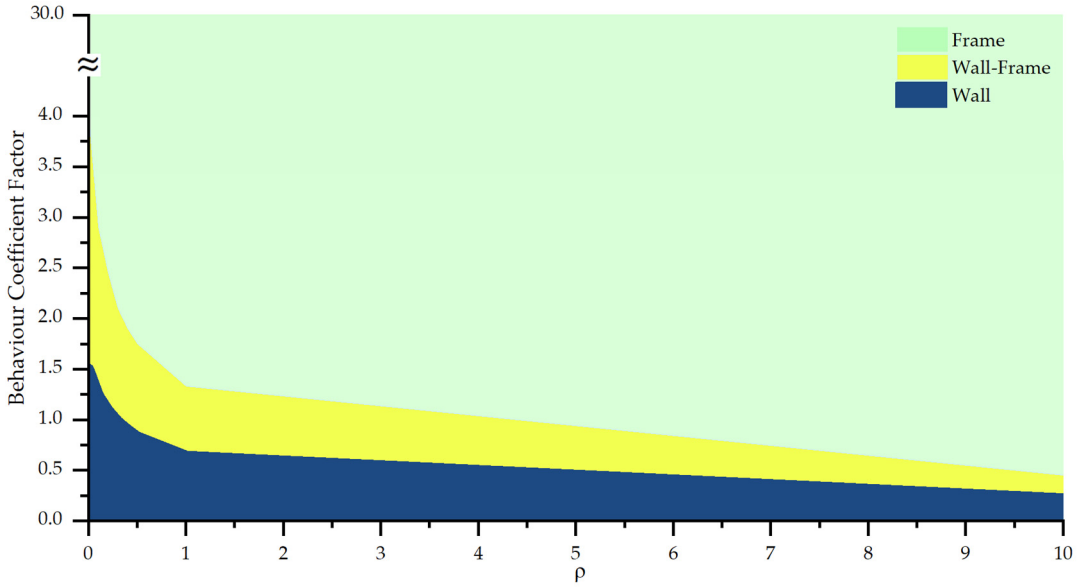

Figure 15. Variation of the structural behavior based on MCR (assumption 2).

6. Conclusions

In this section, the conclusions and results are summarised item by item as follows:

- This study investigates how foundation rotation changes the MCR in buildings whose structural system consists of shear wall frames;
- A sandwich beam model was used to find MCR values. Multi-story buildings are modeled as an equivalent sandwich beam. The differential equations representing this model are written for both static (three different loading cases) and dynamic (single mode) cases, and graphs based on the coefficient of structural behavior and foundation rotation ratio are created for practical use;
- With the proposed method, MCR values can be calculated directly from the graphs related to the structural behavior coefficient and foundation rotation ratio, which are calculated depending on the equivalent stiffnesses of the sandwich beam and the equivalent foundation rotation spring;
- With the presented method, it is possible to calculate the MCR value manually with a calculator in a few minutes. In addition, it is possible to reach the results in seconds with very simple software that can be written;
- As a result of the study, it is seen that the moment carried by the shear wall at the base is reduced by transferring to the frame as a result of the rotation under the shear wall, and as a result, the frames are subjected to more stress;
- At the conclusion of the study, it is observed from the examples solved to investigate the suitability of the presented method that the presented approach gives results compatible with the finite element method;
- In addition, within the scope of this study, it is clearly seen from the solved examples that it is sufficient to consider a single mode in finding MCR values in response spectrum analysis, unlike displacements and internal forces;
- A distinctive feature of this work is that it is a method that enables the rapid determination of moment contribution ratios through manual calculations, thus facilitating the analytical process and reducing the dependence on complex calculations;
- The presented method can be used especially in the pre-dimensioning stage and in the order control of the results obtained by the finite element method. Incorrect results can be obtained due to incorrect data entry in finite element analysis software.

With the presented method, possible data entry errors in finite element analysis can be eliminated;

- The method presented in this study is valid for buildings that are symmetrically placed in the plan or, in other words, the translational and torsional movements are unconnected. In future studies, the presented method can be improved for asymmetric buildings;
- The presented method is developed for regular and simple buildings and is not suitable for the analysis of irregular buildings in its current form. However, in future studies, the presented method can be developed for the analysis of irregular buildings;
- Furthermore, by improving the presented method, the change in the MCR ratio in systems that exhibit nonlinear behavior in terms of materials can be taken into account in future studies.

Author Contributions: All authors have contributed equally. All authors have read and agreed to the published version of the manuscript.

Funding: This research received no external funding.

Data Availability Statement: Some or all of the data, models, or code generated or used during this study can be obtained from the corresponding authors upon request.

Conflicts of Interest: The authors declare no conflicts of interest.

References

1. Al Agha, W.; Alozzo Almorad, W.; Umamaheswari, N.; Alhelwani, A. Study the seismic response of reinforced concrete high-rise building with dual framed-shear wall system considering the effect of soil structure interaction. *Mater. Today Proc.* **2021**, *43*, 2182–2188. [CrossRef]
2. Chen, S.; Liu, Q.; Zhai, C.; Wen, W. Influence of building-site resonance and building properties on site-city interaction: A numerical investigation. *Soil. Dyn. Earthq. Eng.* **2022**, *158*, 107307. [CrossRef]
3. Bozdogan, K.B. The effect of foundation elasticity on dynamic behaviour of buildings. *Gradevinar* **2011**, *63*, 335–340.
4. Vicencio, F.; Alexander, N. Numerical analysis of structure-soil-structure interaction for two different buildings during earthquakes. In Proceedings of the 7th International Conference on Computational Methods in Structural Dynamics and Earthquake Engineering, Crete, Greece, 24–26 June 2019.
5. Tong, F.; Christopoulos, C. Insights on higher-mode effects in high-rise buildings with flexible base rotational and translational restraints: A theoretical study using a continuum beam analogy. *J. Earthq. Eng.* **2021**, *27*, 314–339. [CrossRef]
6. Katrangi, M.; Memarpour, M.M.; Yakhchalian, M. Assessment of the seismic performance and the base shear contribution ratios of the RC wall-frame dual system considering soil–structure interaction. *J. Earthq. Eng.* **2022**, *26*, 5290–5317. [CrossRef]
7. Chandler, M.; Hutchinson, G.L. Torsional coupling effects in the earthquake response of asymmetric buildings. *Eng. Struct.* **1986**, *8*, 222–236. [CrossRef]
8. Perus, I.; Fajfar, P. On the inelastic torsional response of single-storey structures under bi-axial excitation. *Earthq. Eng. Struct. Dyn.* **2005**, *34*, 931–941. [CrossRef]
9. Tahghighi, H.; Mohammadi, A. Numerical evaluation of soil–structure interaction effects on the seismic performance and vulnerability of reinforced concrete buildings. *Int. J. Geomech.* **2020**, *20*, 04020072. [CrossRef]
10. Lou, M.; Wang, H.; Chen, X.; Zhai, Y. Structure–soil–structure interaction: Literature review. *Soil. Dyn. Earthq. Eng.* **2011**, *31*, 1724–1731. [CrossRef]
11. Forcellini, D.A. Novel Framework to Assess Soil Structure Interaction (SSI) Effects with Equivalent Fixed-Based Models. *Appl. Sci.* **2021**, *11*, 10472. [CrossRef]
12. Carbonari, S.; Dezi, F.; Leoni, G. Linear soil–structure interaction of coupled wall–frame structures on pile foundations. *Soil. Dyn. Earthq. Eng.* **2011**, *31*, 1296–1309. [CrossRef]
13. Carbonari, S.; Dezi, F.; Leoni, G. Nonlinear seismic behaviour of wall-frame dual systems accounting for soil-structure interaction: Nonlinear behaviour of wf systems with soil-structure interaction. *Earthq. Eng. Struct. Dyn.* **2012**, *41*, 1651–1672. [CrossRef]
14. Santrač, P.; Grković, S.; Kukaras, D.; Đuric, N.; Svilar, M. Case study—An extreme example of soil–structure interaction and the damage caused by works on foundation strengthening. *Appl. Sci.* **2021**, *11*, 5201. [CrossRef]
15. Jiménez, G.A.L.; Dias, D. Dynamic soil–structure interaction effects in buildings founded on vertical reinforcement elements. *CivilEng* **2022**, *3*, 573–593. [CrossRef]
16. Oz, I.; Senel, S.M.; Palanci, M.; Kalkan, A. Effect of soil-structure interaction on the seismic response of existing low and mid-rise RC buildings. *Appl. Sci.* **2020**, *10*, 8357. [CrossRef]
17. Bariker, P.; Kolathayar, S. Dynamic soil structure interaction of a high-rise building resting over a finned pile mat. *Infrastructures* **2022**, *7*, 142. [CrossRef]

18. Wang, J.; Xie, Y.; Guo, T.; Du, Z. Predicting the Influence of Soil–Structure Interaction on Seismic Responses of Reinforced Concrete Frame Buildings Using Convolutional Neural Network. *Buildings* **2023**, *13*, 564. [CrossRef]
19. Shehata, O.E.; Farid, A.F.; Rashed, Y.F. A suggested dynamic soil—Structure interaction analysis. *J. Eng. Appl. Sci.* **2023**, *70*, 63. [CrossRef]
20. Ali, T.; Eldin, M.N.; Haider, W. The Effect of Soil-Structure Interaction on the Seismic Response of Structures Using Machine Learning, Finite Element Modeling and ASCE 7-16 Methods. *Sensors* **2023**, *23*, 2047. [CrossRef]
21. Gan, J.; Li, P.; Liu, Q. Study on dynamic structure-soil-structure interaction of three adjacent tall buildings subjected to seismic loading. *Sustainability* **2019**, *12*, 336. [CrossRef]
22. Forcellini, D. The Role of Soil Structure Interaction on the Seismic Resilience of Isolated Structures. *Appl. Sci.* **2022**, *12*, 9626. [CrossRef]
23. Lanes, R.M.; Greco, M.; Almeida, V.d.S. Viscoelastic Soil–Structure Interaction Procedure for Building on Footing Foundations Considering Consolidation Settlements. *Buildings* **2023**, *13*, 813. [CrossRef]
24. Zhang, X.; Far, H. Effects of dynamic soil-structure interaction on seismic behaviour of high-rise buildings. *Bull. Earthq. Eng.* **2022**, *20*, 3443–3467. [CrossRef]
25. Zhang, X.; Far, H. Seismic behaviour of high-rise frame-core tube structures considering dynamic soil–structure interaction. *Bull. Earthq. Eng.* **2022**, *20*, 5073–5105. [CrossRef]
26. De-la-Colina, J.; Valdés-González, J.; González-Pérez, C.A. Experiments to study the effect of foundation rotation on the seismic building torsional, response of a reinforced concrete space frame. *Eng. Struct.* **2013**, *56*, 1154–1163. [CrossRef]
27. Koboevic, S.; Murugananthan, U.; Reyes-Fernandez, A.; Madani, H.M.; Wiebe, L. Seismic design of foundations for steel-framed buildings: A Canadian perspective. In *Lecture Notes in Civil Engineering, Proceedings of the 10th International Conference on Behaviour of Steel Structures in Seismic Areas, Timisoara, Romania, 25–27 May 2022*; Springer International Publishing: New York, NY, USA, 2023; pp. 1089–1096.
28. Adebar, P. Nonlinear rotation of capacity-protected foundations: The 2015 Canadian building code. *Earthq. Spectra Prof. J. Earthq. Eng. Res. Inst.* **2015**, *31*, 1885–1907. [CrossRef]
29. Ekrami Kakhki, S.; Kheyroddin, A.; Mortezaei, A. Numerical Investigation of the Progressive Collapse of the Reinforced Concrete Wall-Frame Structures Considering the Soil–Structure Interaction. *Int. J. Concr. Struct. Mater* **2023**, *17*, 22. [CrossRef]
30. Sadek, M.; Hage Chehade, F.; Ali, B.; Arab, A. Seismic Soil Structure interaction for Shear wall structures. *MATEC Web Conf.* **2019**, *281*, 02006. [CrossRef]
31. Mohsenian, V.; Nikkhoo, A.; Hejazi, F. An investigation into the effect of soil-foundation interaction on the seismic performance of tunnel-form buildings. *Soil. Dyn. Earthq. Eng.* **2019**, *125*, 105747. [CrossRef]
32. Alexandre, L.D.J.; Mansur, W.J.; Lopes, F.D.R.; Santa Maria, P.E.L.D. Soil-structure interaction with time-dependent behaviour of both concrete and soil. *Lat. Am. J. Solids Struct.* **2022**, *19*. [CrossRef]
33. Tang, Y.; Li, Y.; Jiang, B.; Wang, L.; Ji, S. Study on Redistribution of Internal Force and Plastic Hinge Development of Mountainous Building Structures with Foundations at Two Different Elevations. *Buildings* **2023**, *13*, 909. [CrossRef]
34. Mishra, S.; Samanta, A. Seismic response of multi-storied building with shear wall considering soil-structure interaction in Patna, India. In *Structures*; Elsevier: Amsterdam, The Netherlands, 2023; Volume 56, p. 104877. [CrossRef]
35. Choinière, M.; Paultre, P.; Léger, P. Influence of soil-structure interaction on seismic demands in shear wall building gravity load frames. *Eng. Struct.* **2019**, *198*, 109259. [CrossRef]
36. Noureldin, M.; Ali, T.; Kim, J. Machine learning-based seismic assessment of framed structures with soil-structure interaction. *Front. Struct. Civ. Eng.* **2023**, *17*, 205–223. [CrossRef]
37. Sharma, N.; Dasgupta, K.; Dey, A. Prediction of natural period of RC frame with shear wall supported on soil-pile foundation system using artificial neural network. *J. Earthq. Eng.* **2022**, *26*, 4147–4171. [CrossRef]
38. Requena García de la Cruz, M.V.; Romero Sánchez, E.; Morales Esteban, A. Numerical investigation of the contribution of the soil-structure interaction effects to the seismic performance and the losses of RC buildings. *Dev. Built Environ.* **2022**, *12*, 100096. [CrossRef]
39. Terzi, V.G.; Athanatopoulou, A. Influence of soil structure interaction effects on the real elastic axis of asymmetric buildings. *Soil. Dyn. Earthq. Eng.* **2021**, *146*, 106775. [CrossRef]
40. Jesica, A.; Pudjisuryadi, P.; Rosidi, D. Application of Soil Structure Interaction on Building with Basement using Nonlinear Soil Springs. *Civ. Eng. Dimens.* **2023**, *25*, 20–28. [CrossRef]
41. Toutanji, H.A. The effect of foundation flexibility on the interaction between shear walls and frames. *Eng. Struct.* **1977**, *19*, 1034–1042. [CrossRef]
42. Di, B.; Fu, X. Seismic behaviour of shear wall-frame systems considering foundation stiffness. *Int. J. Struct. Stab. Dyn.* **2017**, *17*, 1740041. [CrossRef]
43. Bozdogan, K.B.; Keskin, E.; Ozturk, D. A Practical Method for Determining Dynamic Characteristics of Buildings Under the Effect of Foundation Rotations. *Int. J. Struct. Stab. Dyn.* **2023**. [CrossRef]
44. Greco, A.; Caddemi, S.; Caliò, I.; Fiore, I. A Review of Simplified Numerical Beam-like Models of Multi-Storey Framed Buildings. *Buildings* **2022**, *12*, 1397. [CrossRef]
45. Piccardo, G.; Tubino, F.; Luongo, A. Equivalent Timoshenko linear beam model for the static and dynamic analysis of tower buildings. *Appl. Math. Model.* **2019**, *71*, 77–95. [CrossRef]

46. Çağatay, I.H.; Güzeldağ, S. *Yeni Deprem Yönetmeliği (TDY-98): SAP 2000N Uygulamaları*; Birsen Yayınevi: Fatih/İstanbul, Turkey, 2002.
47. Duzgun, M.; Tanarslan, H.M. Perde–çerçeveli yapilarda αm perde katki katsayisinin diferansiyel denklem yöntemi ile bulunmasi ve geliştirilen bilgisayar programi. *Dokuz Eylül Üniv. Mühendislik Fakültesi Fen. Mühendislik Derg.* **2003**, *5*, 89–101.